Electron concentration and on-site interaction effects for the spin and charge excitation spectra in the two-dimensional Hubbard model

T. Saikawa and A. Ferraz
Laboratório de Supercondutividade, Centro Internacional de Física da Matéria Condensada, Universidade de Brasília, CEP 70919-970 Brasília-DF, Brazil

(Received 20 October 1997; revised manuscript received 27 January 1998)

Electron concentration and on-site interaction effects for spin and charge excitations in the two-dimensional Hubbard model are investigated. Using the auxiliary boson approach, which takes into account the spin and charge fluctuation effects, we derive an effective model which reproduces qualitatively well electronic states for the weak- and intermediate-coupling Hubbard models. The spin response function shows drastic changes as a function of the interaction and of the electron concentration. For the intermediate coupling regime, the Stoner enhancement around $\mathbf{q}=(\pi,\pi)$ and the spin-density-wave-like collective mode are obtained. In contrast, the charge response function does not have any specific structure for this interaction range. Finally, the electron concentration dependence of the zero sound velocity is discussed for the weak-coupling regime. The zero sound mode is shown to have a specific doping dependence that is associated with the existence of a hopping in the lattice. [S0163-1829(98)06428-5]

I. INTRODUCTION

Electronic states of the Hubbard model have been investigated intensively in many studies[1–11] since the discovery of high-temperature (high-T_c) superconductors. As a result, it is now possible to draw a relatively detailed picture of the single-particle spectrum for that model. The behavior of the spectral function shows dramatic changes as a function of the interaction U, the electron concentration n, and the temperature T. For example, in the doped system, the single-particle density of states has a quasiparticle peak structure at the Fermi energy. For the intermediate- or strong-coupling regime, the density of states has a pseudogap, and, if the system is not doped, there is a Mott-Hubbard gap in any dimension, with the lower and upper Hubbard bands being formed in the negative and positive high-energy regions, respectively.

However, not much is known about the dynamical properties of the response functions in the Hubbard model. Here we focus on the dynamical behavior of the spin and charge response functions in the Hubbard model. Keeping in mind its relation to the high-T_c superconductors, we consider the two-dimensional (2D) Hubbard model, but some results will also hold in higher-dimensional models.

So far, only the spin and charge response functions of the 2D t-J model have been investigated in many works.[12–17] Though the local electron configuration constraint in this model is a strong restriction not always present in the Hubbard model, the properties of the response functions in the t-J model may well give important information which may be generally true for all strongly correlated systems. The following features can be observed in the t-J model: (i) the spin response function has a low-energy sharp peak in the small doping regime, especially around the momentum (π,π); (ii) the charge response function is rather broad in a wide energy range, and no sharp excitation can be observed. In some investigations[1,10,18] on the 2D Hubbard model, the spin and charge response functions show a similar behavior in the low-doping and strong-coupling regimes.

The above-mentioned electronic state evolution must play an important role in characterizing the behavior of the response functions. However, how they precisely relate to each other is still unclear. The reason for this is that interaction effects on the evolution of the dynamical properties of the response functions have not been fully investigated. To clarify these points, in this paper we study both the effects of the electron concentration n and the interaction U in the response functions, by taking into explicit account the evolution of the single-particle spectra.

In our previous work[11] the electronic states of the Hubbard model were investigated numerically using an auxiliary boson approach in which the effects of both the spin and charge fluctuations were considered in an equal footing. The self-energies were calculated up to one-loop order, taking into account the fermion-boson interaction. Although there was a strict restriction on the maximum value of the interaction U due to the Stoner criterion, the obtained spectral function reproduced qualitatively well both the narrow quasiparticle band on the Fermi energy and the lower and upper Hubbard bands.[11]

In this paper, we use the same scheme to investigate the dynamical properties of the spin and charge response functions. The effects of the electron concentration n and the Hubbard interaction U on the dynamical spin and charge response functions are analyzed in detail. In Sec. II, the formulation of our auxiliary boson method is reviewed briefly. An effective fermion-boson model and an important expression needed to describe the electronic states are derived. In Sec. III, the spin and charge response functions are obtained from the effective model. The numerical results showing the evolution of the spin and charge spectra are given in Sec. IV. We find for both the spin and charge spectra a very specific and drastic evolution when we change the electron concentration n and the interaction U. Section V is devoted to concluding remarks. Finally, in the Appendix, we summarize the

doping dependence of the zero sound velocity in the weak-coupling Hubbard model within the conventional random-phase approximation. We find that the zero sound in the Hubbard model has a specific doping dependence which considerably modifies the result obtained for the interacting electron-gas model.

II. MODEL

We consider the standard Hubbard model in a two-dimensional square lattice with a unit lattice constant at zero temperature. In $k=(\mathbf{k},\omega)$ space, the action[11] equivalent to the Hubbard model is

$$S=\sum_{\sigma}\int_{k}\tilde{\Psi}^{\dagger}_{\sigma}(k)(\omega+\mu-\varepsilon_{\mathbf{k}})\tilde{\Psi}_{\sigma}(k) - \frac{U}{2}\sum_{a,b=0}^{3}\int_{q}\tilde{s}^{(a)}(-q)\,\eta_{ab}\tilde{s}^{(b)}(q)\,, \tag{2.1}$$

where $\int_k \equiv \int (d\omega/2\pi)\,[d\mathbf{k}/(2\pi)^2]$, $q=(\mathbf{q},\nu)$, and $\tilde{\Psi}^{\dagger}_{\sigma}(k)$, and $\tilde{\Psi}_{\sigma}(k)$ are the Grassmann fields for the electrons and $\varepsilon_{\mathbf{k}}=-2t(\cos k_x+\cos k_y)$. The last term corresponds to the Hubbard interaction with $\eta_{00}=1$, $\eta_{11}=\eta_{22}=\eta_{33}=-1$ and $\eta_{ab}=0$ for $a\neq b$. We have defined

$$\tilde{s}^{(a)}(q)=\frac{1}{2}\sum_{\sigma,\sigma'}\int_{k}\tilde{\Psi}^{\dagger}_{\sigma}(k+q)\,\tau^{(a)}_{\sigma\sigma'}\tilde{\Psi}_{\sigma'}(k)\,, \tag{2.2}$$

where the $\tau^{(a)}$'s are Pauli matrices with $a=1$, 2, and 3, and $\tau^{(0)}$ is the 2×2 unit matrix.[11]

We next introduce four auxiliary bosonic operators $\tilde{\phi}^{(a)}(q)$ for the charge ($a=0$) and the spin ($a=1,2,3$) channels through an appropriate Hubbard-Stratonovich transformation.[11] The following effective action is thus obtained:

$$S_{\mathrm{eff}}=\sum_{\sigma}\int_{k}\tilde{\Psi}^{\dagger}_{\sigma}(k)(\omega+\mu-\varepsilon_{\mathbf{k}})\tilde{\Psi}_{\sigma}(k) + \frac{1}{2}\sum_{a,b=0}^{3}\int_{q}\tilde{\phi}^{(a)}(-q)\,\eta_{ab}\tilde{\phi}^{(b)}(q) + \sum_{a,b=0}^{3}\int_{q}\tilde{\phi}^{(a)}(-q)\,\eta_{ab}\sqrt{U}\tilde{s}^{(b)}(q)\,. \tag{2.3}$$

Integrating out the Grassmann fields, we have that

$$S'_{\mathrm{eff}}(\tilde{\phi})=\frac{1}{2}\sum_{a,b=0}^{3}\int_{q}\tilde{\phi}^{(a)}(-q)\,\eta_{ab}\tilde{\phi}^{(b)}(q) - i\,\mathrm{tr}\,\ln[\mathbf{M}(\tilde{\phi})]\,, \tag{2.4}$$

where $\mathbf{M}$ is defined by

$$[\mathbf{M}(\tilde{\phi})]_{k\sigma,k'\sigma'}=(\omega+\mu-\varepsilon_{\mathbf{k}})\,\delta_{k,k'}\delta_{\sigma,\sigma'} + \sum_{a=0}^{3}\tilde{\phi}^{(a)}(k-k')\,\frac{\sqrt{U}}{2}\,\eta_{aa}\tau^{(a)}_{\sigma\sigma'}\,. \tag{2.5}$$

Taking into account the fluctuations of the boson fields, we can expand the effective action around the saddle-point solution. Here we use the saddle-point solutions $\phi_0^{(0)}=-\sqrt{U}n/2$ for $a=0$ and $\phi_0^{(a)}=0$ for $a\neq 0$. The electron number n is calculated from

$$n=-i\sum_{\sigma}\int_{k}G_0(k), \tag{2.6}$$

where the saddle-point Green's function is defined by

$$G_0(k)=\frac{1}{\omega+\mu_0-\varepsilon_{\mathbf{k}}+i\,\eta\,\mathrm{sgn}(\omega)}. \tag{2.7}$$

The chemical potential $\mu_0=\mu-Un/4$ is determined consistently with the given electron concentration n.

The second-order term of the S'_{eff} expansion can be written as

$$S'_2=\frac{1}{2}\sum_{a=0}^{3}\int_{q}\delta\tilde{\phi}^{(a)}(-q)D_{aa}(q)^{-1}\delta\tilde{\phi}^{(a)}(q), \tag{2.8}$$

with the boson propagator determined by

$$D_{aa}(q)^{-1}=\eta_{aa}+\frac{U}{2}\chi_0(q), \tag{2.9}$$

where $\chi_0(q)$ is given by

$$\chi_0(q)=i\int_{k}G_0(k+q)G_0(k). \tag{2.10}$$

For a paramagnetic state, each spin component contributes equally to $D_{aa}(q)$.

To calculate the Green's function beyond the saddle-point approximation, we consider a new fermion-boson action S''_{eff}, taking $D_{aa}(q)$ as the zeroth-order boson propagator:

$$S''_{\mathrm{eff}}=\sum_{\sigma}\int_{k}\tilde{\Psi}^{\dagger}_{\sigma}(k)(\omega+\mu-\varepsilon_{\mathbf{k}})\tilde{\Psi}_{\sigma}(k) + \frac{1}{2}\sum_{a=0}^{3}\int_{q}\delta\tilde{\phi}^{(a)}(-q)D_{aa}(q)^{-1}\delta\tilde{\phi}^{(a)}(q) + \sum_{a=0}^{3}\sum_{\sigma,\sigma'}\int_{k}\int_{q}\delta\tilde{\phi}^{(a)}(q)\,\frac{\sqrt{U}}{2}\,\eta_{aa} \times\tilde{\Psi}^{\dagger}_{\sigma}(k+q)\,\tau^{(a)}_{\sigma\sigma'}\tilde{\Psi}_{\sigma'}(k)\,. \tag{2.11}$$

We can easily establish the Feynman rules for this effective action. Up to one-loop order, the fermion Green's function can be written as

$$G(k)^{-1}=\omega+\mu_*-\varepsilon_{\mathbf{k}}-i\frac{U}{4}\sum_{a=0}^{3}\int_q G_0(k+q)D_{aa}(q)\,, \tag{2.12}$$

where the chemical potential μ_* is determined consistently with the electron concentration n. The U-dependent term above is the one-loop fermion self-energy for both the spin and charge components.

III. SPIN AND CHARGE RESPONSE FUNCTIONS

We define the spin ($\alpha=s$) and charge ($\alpha=c$) retarded response functions χ_α (Ref. 22) as

$$\chi_s(\mathbf{q},t-t')=i\theta(t-t')\langle[m^{(z)}(\mathbf{q},t),m^{(z)}(-\mathbf{q},t')]\rangle \tag{3.1}$$

and

$$\chi_c(\mathbf{q},t-t')=i\theta(t-t')\langle[n(\mathbf{q},t),n(-\mathbf{q},t')]\rangle\,, \tag{3.2}$$

where $m^{(z)}(\mathbf{q},t)$ and $n(\mathbf{q},t)$ are the $(\mathbf{q},t)$ representation of

$$m^{(z)}(\mathbf{r},t)=\sum_\sigma \mathrm{sgn}(\sigma)\Psi_\sigma^\dagger(\mathbf{r},t)\Psi_\sigma(\mathbf{r},t) \tag{3.3}$$

and

$$n(\mathbf{r},t)=\sum_\sigma \Psi_\sigma^\dagger(\mathbf{r},t)\Psi_\sigma(\mathbf{r},t)\,. \tag{3.4}$$

Following the same scheme used above to derive the fermion Green's function, we perturbatively expand the response function χ_α. The zeroth-order term of χ_α gives only the noninteracting polarization function $P_0(q)\equiv 2\chi_0(q)$. To simplify the calculation, we take no account of vertex corrections, at this stage.

However, in the series expansion for $\chi_\alpha(q)$, we have to avoid the double counting of the noninteracting polarization bubble $\chi_0(q)$. This is due to the fact that the boson line itself already includes the one-loop polarization $\chi_0(q)$ to infinite order, as is indicated by Eq. (2.9). For this, it is useful to introduce the renormalized polarization function $\Pi(q)$ given in terms of the corresponding renormalized single-particle Green's functions. That is, $\Pi(q)$ is given by

$$\Pi(q)=i\int_k G(k+q)G(k)\,. \tag{3.5}$$

We can write the expansion of $\chi_\alpha(q)$ diagrammatically, as shown in Fig. 1(a). By subtracting $P_0(q)$ from $P(q)=2\Pi(q)$ in the intermediate diagram, as shown in the rectangular brackets of Fig. 1(a), we automatically take into account the elimination of all diagrams which contain doubly counted $\chi_0(q)$. The full Green's function is represented in Fig. 1(b). From the figure, we can write

$$\chi_\alpha=P-PV_\alpha P+PV_\alpha(P-P_0)V_\alpha P - PV_\alpha(P-P_0)V_\alpha(P-P_0)V_\alpha P+\cdots, \tag{3.6}$$

where $V_\alpha(q)\equiv(U/4)D_\alpha(q)$, the sign of each term being determined by the number of fermion loops. Here, for simplicity, the boson propagators have been redefined by introducing the subscript α, where $\alpha=s$ or c, instead of $a=1$, 2, and 3 or $a=0$. Thus $D_\alpha^{-1}=\eta_\alpha+(U/2)\chi_0(q)$ with $\eta_s\equiv-1$ and $\eta_c\equiv 1$, and we have

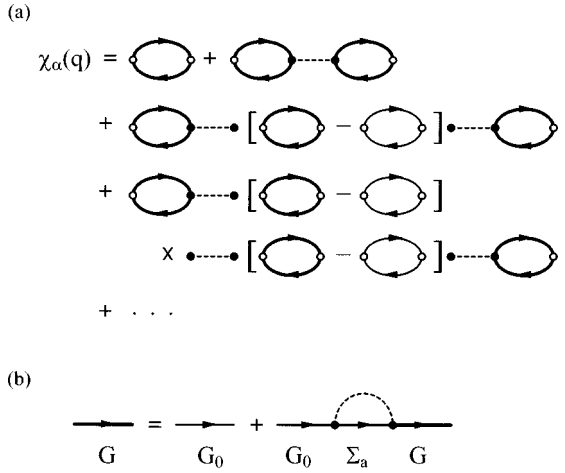

FIG. 1. Diagram representations of (a) the expansion series of the response functions $\chi_\alpha(q)$ and (b) the Dyson equation of the fermion Green's function $G(k)$. The solid line, thick solid line, and dashed line represent $G_0(k)$, $G(k)$, and $D_\alpha(q)$, respectively.

$$\chi_\alpha=P-P\frac{V_\alpha}{1+(P-P_0)V_\alpha}P\,. \tag{3.7}$$

Thus, the charge and spin response functions can be written as

$$\chi_\alpha(q)=\frac{2\Pi(q)}{1+\eta_\alpha(U/2)\,\Pi(q)}. \tag{3.8}$$

The denominator of Eq. (3.8) has a factor $U/2$ which is different from the standard random-phase-approximation (RPA) expression. It produces a shift from the standard RPA even in the weak-coupling limit. The difference originates in the interaction term of our four-auxiliary-boson approach shown in Eq. (2.3). The coupling constant of the boson-fermion interaction term is $\sqrt{U/4}$ in our four-auxiliary-boson approach. The numerical factor in general depends on the number of auxiliary bosons.[19,20] If we consider n bosons, the corresponding boson-fermion coupling is $\sqrt{U/n}$, and the factor in the χ_α denominator becomes $2U/n$. This latter factor of 2 is produced by the spin summation in the fermion loops. Since in our case there are four bosons, we arrive at the factor $U/2$. The denominator factor in the boson propagator D_α has the same origin.

The spectra of the spin ($\alpha=s$) and charge ($\alpha=c$) response functions are defined by the corresponding imaginary part of $\chi_\alpha(q)$ as

$$\mathrm{Im}\;\chi_\alpha(q)=\frac{2\,\mathrm{Im}\,\Pi(q)}{(1+\eta_\alpha(U/2)\mathrm{Re}\;\Pi(q))^2+(U/2\,\mathrm{Im}\;\Pi(q))^2}, \tag{3.9}$$

with

$$\text{Im}\,\Pi(q)=\int_k [1-\text{sgn}(\omega+\nu)\text{sgn}(\omega)]\text{Im}\,G(k+q)\text{Im}\,G(k)\,, \tag{3.10}$$

and $\text{Re}\,\Pi(q)$ being calculated from $\text{Im}\,\Pi(q)$ by the Kramers-Kronig transformation.

Note that we neglected all vertex corrections to avoid further numerical difficulty. Although with such an approximation we might lose some processes produced by vertex corrections, this scheme is useful, and it is the simplest one available in order to investigate directly the effect of the spectral functions in the response function. One shortcoming of this approach is the violation of the spin and charge conservation denoted by $\text{Im}\,\chi_\alpha(\mathbf{q}=0,\omega)=0$. In our calculation, however, the intensity of $\text{Im}\,\chi_\alpha(\mathbf{q}\sim 0,\omega)$ is sufficiently small in comparison with the results obtained for other $\mathbf{q}$ values. Thus, it does not give any essential modification in all the results from this work.

In our formulation we take into account the one-loop fermion and boson self-energies in the fermion Green's function $G(k)$ and the boson propagator $D_\alpha(q)$. We also consider the dressed one-loop bubble diagram as the irreducible polarization function in the spin and charge response functions. In this respect our approximation reminds one of the so-called fluctuation exchange (FLEX) approximation,[1,21] that also takes into account the dressed one-loop diagram. In their treatment both Green's function and one-loop dressed fermion bubble are obtained perturbatively in a self-consistent manner. Our method is a combined nonperturbative and perturbative treatment. We use the noninteracting one-loop bubble in our nonperturbatively derived boson propagators. This makes our scheme totally different from the FLEX approximation.

IV. NUMERICAL RESULTS

A. *U* dependence of the response functions

In Figs. 2 and 3, we show the contour line plot drawn with the numerical results of the U dependence of the spin and charge response functions for a fixed electron concentration $n=0.8$. For $U/t=0$, both response functions are determined by the imaginary part of the noninteracting one-loop polarization function written as

$$\text{Im}\,P_0(q)=2\,\text{Im}\,\chi_0(q)=2\pi\,\text{sgn}(\nu)\sum_{\mathbf{k}}\,[\,\theta(\varepsilon_{\mathbf{k}+\mathbf{q}}-\mu)-\theta(\varepsilon_{\mathbf{k}}-\mu)]\delta(\nu-\varepsilon_{\mathbf{k}+\mathbf{q}}+\varepsilon_{\mathbf{k}})\,. \tag{4.1}$$

From Fig. 2(a), we find that $\text{Im}\,P_0(q)$ has two different characteristic properties. One is manifest in the region around the zone corner (π,π). $\text{Im}\,P_0(q)$ at $\mathbf{q}=(\pi,\pi)$ can be written as

$$\text{Im}\,P_0(\mathbf{q}=(\pi,\pi),\nu)=2\pi\sum_{\mathbf{k}}\,\delta(\nu+2\varepsilon_{\mathbf{k}})\,, \tag{4.2}$$

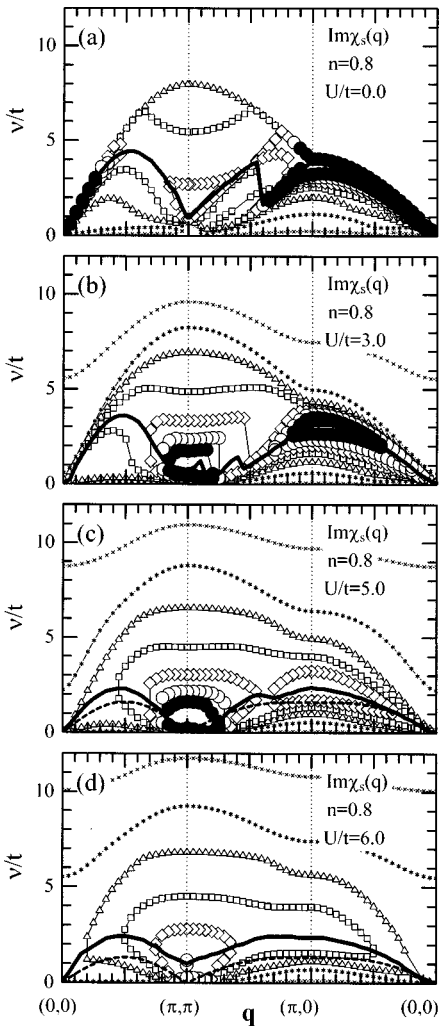

FIG. 2. Contour plot of the U dependence of the dynamical spin response function $\text{Im}\,\chi_s(q)$ at $n=0.8$, for (a) $U/t=0$, (b) 3.0, (c) 5.0, and (d) 6.0. Sequence of symbols represent an equal intensity line of $\text{Im}\,\chi_s(q)$. The symbols $\times$, *, triangle, square, diamond, circle, and solid circle correspond to $\text{Im}\,\chi_s(q)=0.02$, 0.1, 0.2, 0.3, 0.4, 0.5, and 0.6, respectively. The thick curve represents maximum intensity points. There is one maximum point for each $\mathbf{q}$ value. Thick dashed curves in (c) and (d) represent the SDW dispersion relation for $U/t=5.0$ and 6.0, respectively.

where $\nu>2|\mu|$ for $\nu>0$. Apart from the low-energy gap in the region $0<\nu<2|\mu|$, the right-hand side is equivalent to the density of states of the tight-binding band with the nearest-neighbor hopping $2t$.

The second property is the existence of the sharp peak structures near the upper limit of the particle-hole excitation energy around $\mathbf{q}=(0.1\pi,0.1\pi)\sim(0.5\pi,0.5\pi)$ for $\mathbf{q}$ in the (1,1) direction, and also for all $\mathbf{q}$'s in the (1,0) direction. To understand that structure we shall rewrite the integration of Eq. (4.1) into the contour integral

$$\text{Im}\,P_0(q)=2\pi\,\text{sgn}(\nu)\int_{\nu=\varepsilon_{\mathbf{k}+\mathbf{q}}-\varepsilon_{\mathbf{k}}}\times\frac{dl_{\mathbf{k}}}{(2\pi)^2}\,\frac{\theta(\varepsilon_{\mathbf{k}+\mathbf{q}}-\mu)-\theta(\varepsilon_{\mathbf{k}}-\mu)}{|\nabla_{\mathbf{k}}(\varepsilon_{\mathbf{k}+\mathbf{q}}-\varepsilon_{\mathbf{k}})|}\,. \tag{4.3}$$

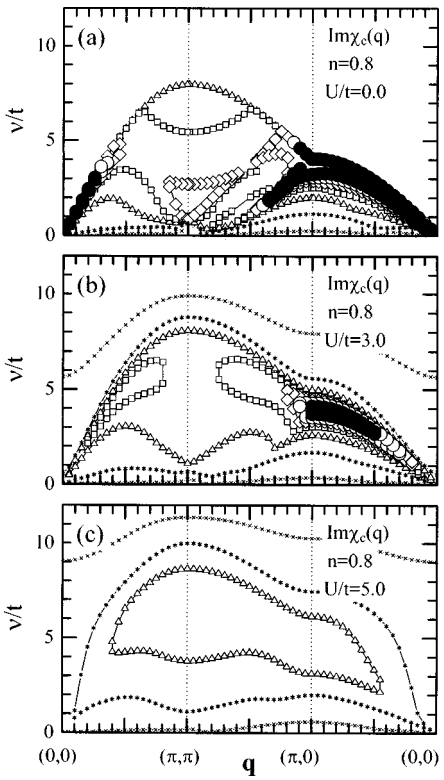

FIG. 3. Contour plot of the U dependence of the dynamical charge response function Im $\chi_c(q)$ at $n=0.8$, for (a) $U/t=0$, (b) 3.0, and (c) 5.0. The meanings of symbols are the same as in Fig. 3.

The peak of Im $P_0(q)$ in the (1,1) direction comes from the contribution near the singularity pole of the integrand $1/|\nabla_{\mathbf{k}}(\varepsilon_{\mathbf{k}+\mathbf{q}}-\varepsilon_{\mathbf{k}})|$ and the particle-hole condition $\theta(\varepsilon_{\mathbf{k}+\mathbf{q}}-\mu)-\theta(\varepsilon_{\mathbf{k}}-\mu)\neq 0$. The pole corresponds to the excitation between $\mathbf{k}+\mathbf{q}=(\pi/2+q_x/2,\pi/2+q_y/2)$ and $\mathbf{k}=(\pi/2-q_x/2,\pi/2-q_y/2)$, which has the excitation energy $\nu(\mathbf{q})=4t[\sin(q_x/2)+\sin(q_y/2)]$. This excitation takes place for dopings near the half-filling, because it goes across a boundary which is the Fermi surface (line) at half-filling. As the electron concentration decreases away from half-filling, this excitation process is forbidden because it violates the particle-hole condition. The small momentum-transfer ($\mathbf{q}\sim 0$) processes are very sensitive to this restriction, since these processes are quickly excluded outside the Fermi surface as electron concentration decreases. Though the above-mentioned pole is located within the range of validity of the particle-hole condition for large $\mathbf{q}$'s, no sharp peak is observed due to the quick decrease of Im $P_0(q)$.

With a similar analysis, we can see that the origin of the peak structure in the (1,0) direction is the pole of $1/|\nabla_{\mathbf{k}}(\varepsilon_{\mathbf{k}+\mathbf{q}}-\varepsilon_{\mathbf{k}})|$. We choose $\mathbf{q}=(q_x,0)$. The excitation process associated with the pole is again the transition between $\mathbf{k}+\mathbf{q}=(\pi/2+q_x/2,k_y)$ and $\mathbf{k}=(\pi/2-q_x/2,k_y)$ with excitation energy $\nu(\mathbf{q})=4t\sin(q_x/2)$, where k_y is chosen arbitrarily within the particle-hole condition. Because of this arbitrariness of k_y, the peak of Im P_0 for the (1,0) direction is sharper than that for the (1,1) direction. Thus, in the finite interaction case, the peak structure in the (1,0) direction is more stable against the incoherent single-particle spectral effect than the peak in the (1,1) direction. We will find this trend in the results obtained next for appropriate values of U.

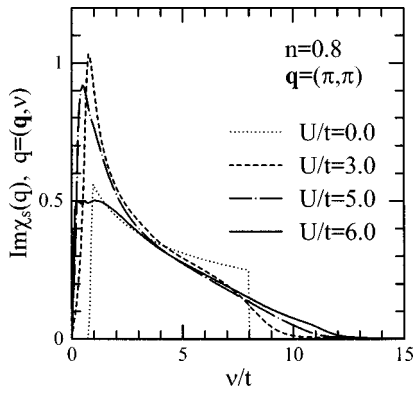

FIG. 4. U dependence of the dynamical spin response function Im $\chi_s(q)$ for $\mathbf{q}=(\pi,\pi)$ at a fixed electron concentration $n=0.8$.

Note that the properties obtained for $U=0$ are associated with the original structure that can be completely determined by the noninteracting band structure, or, in other words, that can be determined by the nature of the nearest-neighbor hopping in the 2D square lattice without interactions.

Figures 2(b)–2(d) show the nonzero U results. As U increases, the above-mentioned sharp structures are broadened. However, for $U/t=3.0$, the corresponding structures still remain to some extent intact, especially the peak structures in the (1,0) direction. Finally, at $U/t=6.0$, no corresponding structure can be seen. This is produced by the broadenings of the incoherent part of the spectral function $A(k)=-(1/\pi)\mathrm{sgn}(\omega)\mathrm{Im}\,G(k)$ in the high-energy region.

The thick curve in Fig. 2 indicates the sequence of the maximum intensity points, one for each $\mathbf{q}$, of Im $\chi_s(q)$. It can be seen that, as U/t increases, the curve is modified and moved to the low-energy regime. That can be interpreted as the formation of the low-energy collective mode, i.e., the spin-density wave (SDW). For comparison with our numerical data, we draw the SDW band dispersion [dashed curve in Figs. 2(c) and 2(d)] $\nu_{\mathrm{SDW}}(\mathbf{q})=2J\sqrt{1-[\varepsilon_{\mathbf{q}}/(4t)]^2}$ derived from the 2D antiferromagnetic Heisenberg model with the Holstein-Primakoff transformation.[23] Here $J\sim 4t^2/U$ and $\varepsilon_{\mathbf{q}}=-2t(\cos q_x+\cos q_y)$. Though this analytical band dispersion may be valid for sufficiently small dopings and for the large coupling regime, the agreement with our data is fine. The difference between ν_{SDW} and our data is due to the effect of the finite doping concentration ($\delta=1-n=0.2$) in our calculation.

Around $\mathbf{q}\sim(\pi,\pi)$ in Im $\chi_s(q)$, we observe the sharp peak structure that is already present for $U/t=3.0$. This Stoner enhancement is a genuine many-body collective excitation. To observe this in detail, in Fig. 4 we show the evolution of Im $\chi_s(q)$ at $\mathbf{q}=(\pi,\pi)$. The Stoner excitation is well enhanced up to $U/t=5.0$. For $U/t=6.0$, we are close to the Stoner instability condition in the boson propagator $D_s(q)$, and the low-energy intensity of Im $\chi_s(q)$ is reduced. This originates in the decrease of the low-energy quasiparticle weight in the single-particle spectra for the finite doping regime as we obtained in our previous work.[11] The tail of the excitation spectrum is spread toward the high-energy region as U/t increases. This behavior is correlated with the developing of the tail in the single-particle electronic states.[11]

The U dependence of the charge response functions are shown in Fig. 3. As in the case of the spin response function,

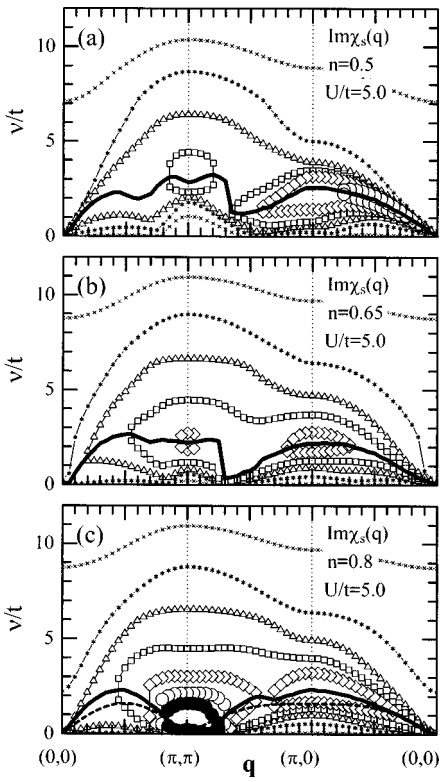

FIG. 5. Contour plot of the n dependence of the dynamical spin response function Im $\chi_s(q)$ at $U/t=5.0$, for (a) $n=0.5$, (b) 0.65, and (c) 0.8. The symbols used are the same as in Fig. 3. Thick curve represents maximum intensity points. As before, for each $\mathbf{q}$ there is one appropriate maximum point. The thick dashed curve in (c) represents the SDW dispersion relation for $U/t=5.0$.

the sharp peak structures on the upper limit of the particle-hole continuum become structureless as U/t increases. The broad weak peak can be seen around $\mathbf{q}=(\pi,\pi)$, and the broad nature is well spread over a wide $\mathbf{q}$ range. Because of the quick development of the incoherent tail above the particle-hole continuum, no collective mode is observed. However, as is well known, the system described within the Landau-Fermi liquid picture must have a zero sound mode at small $\mathbf{q}$ regions. In the Appendix, we discuss the doping dependence of the zero sound mode in the weak-coupling Hubbard model using the conventional RPA framework. We found that the zero sound velocity in the small electron concentration n increases rapidly as n increases, and that it has no $\mathbf{q}$ direction dependence. Contrary to this, in the large n region near half-filling, the zero sound velocity does not depend on n, and has a large $\mathbf{q}$ direction dependence.

B. Doping dependence of the response functions

Figure 5 shows the doping dependence evolution of the response functions for fixed interaction $U/t=5.0$. At $n=0.5$, a clear peak structure can be observed in the (1,0) direction of $\mathbf{q}$. This structure is weakened at $n=0.65$, since the self-energy effect becomes larger as the electron concentration increases. At $n=0.8$, this structure seems to be recovered again, but this is the collective effect similar to the Stoner enhancement. The gap structure in the low-energy region at $\mathbf{q}=(\pi,\pi)$ is gradually buried as n increases. Another gaplike (pseudogap) structure can be seen in the (1,1) direction. It has a bell-shaped structure with its top point around $\mathbf{q}=(\pi/2,0)$. It looks as if this structure is shifted toward the sharp peak in the (1,0) direction. As n increases, this pseudogap is smeared, and a new pseudogap appears with a maximum gap at $\mathbf{q}=(\pi,0)$. This new pseudogap formation is related to the development of the spin collective mode (SDW) which will be discussed below. A similar trend can be seen in the results of the quantum Monte Carlo simulation.[10]

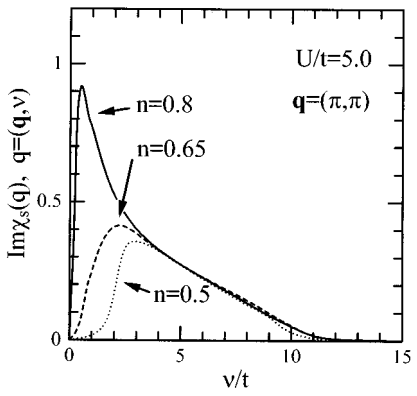

FIG. 6. n dependence of the dynamical spin response function Im $\chi_s(q)$ at $U/t=5.0$ and $\mathbf{q}=(\pi,\pi)$.

At $n=0.5$, a weak peak structure is seen around $\mathbf{q}=(\pi,\pi)$. This structure becomes sharper and moves toward the low-energy region as n becomes larger in the small doping regime. Finally, at $n=0.8$ the strong Stoner enhancement peak arises. Figure 6 shows the development of the Stoner enhancement at $\mathbf{q}=(\pi,\pi)$. A low-energy enhancement peak is drastically produced, but the high-energy behavior is not sensitive to the change of the electron concentration. This strong enhancement in the dynamical spin response functions at $\mathbf{q}=(\pi,\pi)$ is also seen in the earlier FLEX approximation work.[1]

The thick curve in Fig. 5 shows the maximum intensity of $\mathrm{Im}\chi_s$. The curve has a drastic change, i.e., the spin collective mode (SDW) is formed as n approaches the small doping toward half-filling.

Figure 7 shows the evolution of the charge response function for the fixed value $U/t=5.0$. At $n=0.5$, peak structures can be seen in the (1,1) direction around $\mathbf{q}=(0,0)$, and in the (1,0) direction. As already discussed above, they are the traces of the particle-hole excitation in the noninteracting polarization function. These structures are easily smeared and finally disappear as n increases. Roughly speaking, there are two structures at $n=0.5$; the relatively broad high-energy peak around $\mathbf{q}=(\pi,\pi)$, and the sharp peak in the (1,0) direction. The latter originates in the structure of the noninteracting one-loop polarization function $\mathrm{Im}P_0(q)$. As n increases, these two structures are connected and become a single broad structure which is mainly located in the high-energy region around $\nu/t=6-7$. As previously pointed out, the spin response function shows similar emerging behavior, but that can be interpreted in terms of the formation of the SDW dispersion.

V. CONCLUDING REMARKS

In this paper, we investigated the dynamical properties of the spin and charge response functions in the 2D Hubbard

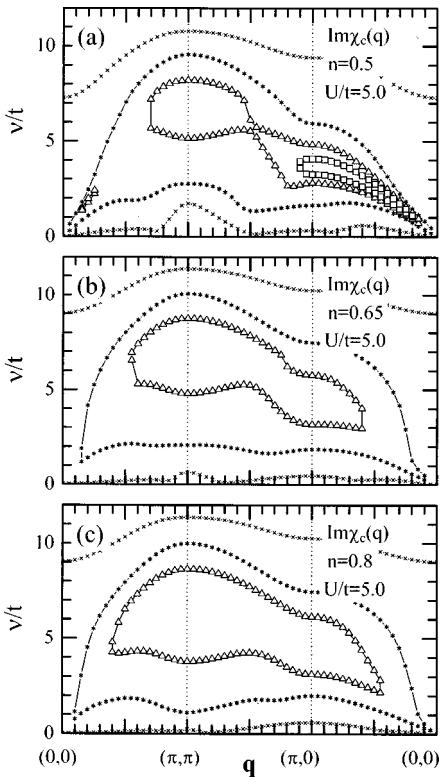

FIG. 7. Contour plot of the n dependence of the dynamical charge response function Im $\chi_c(q)$ at $U/t=5.0$, for (a) $n=0.5$, (b) 0.65, and (c) 0.8. The symbols are the same as in Fig. 3.

model by varying the interaction energy U/t and the electron concentration n. To calculate the dynamical spin and charge response functions, we have used an effective model which makes use of the Hubbard-Stratonovich auxiliary bosons associated with the spin and charge fluctuations coupled with the fermion field. The one-loop order self-energies were taken into account both in the boson propagator and the fermion Green's function.

For $n=0.8$, as U/t increases, low-energy antiferromagnetic Stoner enhancement around $\mathbf{q}=(\pi,\pi)$ is enhanced up to the intermediate-coupling regime. When this takes place, SDW-like dispersion formation is observed. As U/t approaches the Stoner instability criterion, the Stoner enhancement weakens because of the decrease in the quasiparticle weight in the low-energy region around the Fermi energy. Such a decrease is associated with the formation of the pseudogap.

The sharp peak structure located around the upper limit of the particle-hole continuum in the noninteracting case becomes broader and structureless as U/t increases. Furthermore, the tail structure spreads toward the high-energy regime. Both these broadening features can be explained in terms of the incoherent structure in the single-particle spectrum.

Using a slave-boson technique, Khaliullin and Horsh[17] have obtained a low-**q** collective mode which has a broad peak especially for the (1,0) direction in the charge response function of the t-J model. A similar low-**q** mode in the charge response function of the Hubbard model can also be seen in the quantum Monte Carlo (QMC) simulation by Preuss *et al.*[10] In our calculation, the charge response function becomes completely broad, and no clear collective mode is seen. It is not certain that this collective mode exists in the Hubbard model. However, if it does, it might be produced by some vertex correction neglected in the present work.

In conclusion, our formulation takes into account two main features in the response functions. They are the incoherent and coherent properties of the single-particle spectral function and the Stoner-like enhancement factor. By considering those two properties, we can explain the doping and interaction dependences of the dynamical spin and charge response functions. Our approach reproduces rather well the doping dependence obtained in the QMC simulation.[10]

ACKNOWLEDGMENTS

The authors would like to thank S. L. Garavelli, P. E. de Brito, S. Gluzman, and H. Kaga for useful discussions. This work was supported by the Conselho Nacional de Desenvolvimento Científico e Tecnológico (CNPq) and by the Financiadora de Estudos e Projetos (FINEP). Most of the numerical calculations in this work were performed with the supercomputing system at the Institute for Materials Research, Tohoku University, Japan.

APPENDIX: DOPING DEPENDENCE OF THE ZERO SOUND VELOCITY IN THE WEAK-COUPLING HUBBARD MODEL

In this appendix, we discuss the doping effects of the zero sound velocity in the Hubbard model using the standard random-phase approximation (RPA). Our reference model is the two-dimensional Hubbard model with weak on-site Coulomb interaction. In this interaction regime, the RPA is applicable to analyze the charge response function of this model. In this approximation, the charge response function can be written as

$$\chi_{\mathrm{RPA}}(q)=\frac{2\chi_0(q)}{1+U\chi_0(q)} \tag{A1}$$

where $\chi_0(q)$ is defined by Eq. (2.10). The charge excitation is given by

$$\mathrm{Im}\,\chi_{\mathrm{RPA}}(q)=\frac{2\,\mathrm{Im}\,\chi_0(q)}{[1+U\ \mathrm{Re}\,\chi_0(q)]^2+[U\ \mathrm{Im}\ \chi_0(q)]^2}. \tag{A2}$$

This approximation describes the particle-hole excitations and also the collective modes for sufficiently weak coupling.

The collective mode in the charge response function for the energy range above the particle-hole excitation can be obtained as a solution of the following equation within the RPA,

$$1+U\ \mathrm{Re}\,\chi_0(q)=0. \tag{A3}$$

Performing the frequency integration, we have

$$1+U\sum_{\mathbf{k}}\frac{\theta(\varepsilon_{\mathbf{k}}-\mu)-\theta(\varepsilon_{\mathbf{k}+\mathbf{q}}-\mu)}{\nu-\varepsilon_{\mathbf{k}+\mathbf{q}}+\varepsilon_{\mathbf{k}}}=0. \tag{A4}$$

To study the velocity of the zero sound mode which can be expected to exist near the zero momentum, we expand the above expression around $|\mathbf{q}|\approx 0$, where $|\mathbf{q}|=(q_x^2+q_y^2)^{1/2}$, immediately obtaining

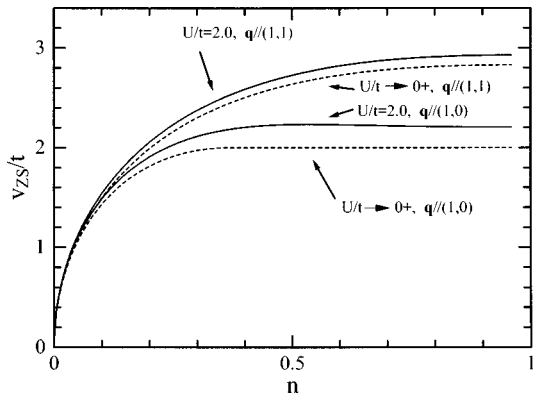

FIG. 8. Electron concentration dependence of the zero sound velocity v_{ZS} within the RPA calculated for $U/t=2.0$ (solid curve) and $U/t\rightarrow 0+$ (dashed curve).

$$1-U\sum_{\mathbf{k}}\frac{\delta(\varepsilon_{\mathbf{k}}-\mu)(\partial\varepsilon_{\mathbf{k}}/\partial\mathbf{k})\cdot\mathbf{q}}{\nu-(\partial\varepsilon_{\mathbf{k}}/\partial\mathbf{k})\cdot\mathbf{q}}=0. \tag{A5}$$

By performing the integration of the δ function, we have the following contour integral:

$$U\int_{\varepsilon_{\mathbf{k}}=\mu}\frac{dl_{\mathbf{k}}}{(2\pi)^2|\nabla_{\mathbf{k}}\varepsilon_{\mathbf{k}}|}\frac{(\partial\varepsilon_{\mathbf{k}}/\partial\mathbf{k})\cdot\mathbf{q}}{\nu-(\partial\varepsilon_{\mathbf{k}}/\partial\mathbf{k})\cdot\mathbf{q}}=1. \tag{A6}$$

The solution of this integral equation determines the zero sound velocity v_{ZS} that can be defined as

$$v_{\mathrm{ZS}}(\mathbf{q}/|\mathbf{q}|)\equiv\frac{\nu}{|\mathbf{q}|}, \tag{A7}$$

dependent on the direction of momentum $\mathbf{q}$.

In Fig. 8, we show the electron concentration n dependence of the zero sound velocity v_{ZS} for the (1,1) and (1,0) directions of $\mathbf{q}$. In the dilute electron concentration regime ($n\sim 0$), the zero sound velocity increases rapidly as the electron concentration n increases. In addition, the two curves for the (1,0) and (1,1) directions overlap almost completely, indicating that the zero sound velocity does not depend on the direction of $\mathbf{q}$ in the large doping regime.

That can be proved as follows. In the dilute limit, the band dispersion can be approximated by

$$\varepsilon_{\mathbf{k}}\sim -4t+2t(k_x^2+k_y^2). \tag{A8}$$

Then the contour equation of the line integral becomes

$$-4t+2t(k_x^2+k_y^2)=\mu \tag{A9}$$

or, in polar coordinates,

$$\begin{aligned} k_x&=\sqrt{2+\mu/2t}\cos\theta,\\ k_y&=\sqrt{2+\mu/2t}\sin\theta, \end{aligned} \tag{A10}$$

where θ can vary from 0 to 2π. It also follows that

$$|\nabla_{\mathbf{k}}\varepsilon_{\mathbf{k}}|=4t\sqrt{2+\mu/2t}. \tag{A11}$$

Then, by introducing

$$\begin{aligned} q_x&=|\mathbf{q}|\cos\alpha,\\ q_y&=|\mathbf{q}|\sin\alpha, \end{aligned} \tag{A12}$$

Eq. (A6), which determines the zero sound velocity, becomes

$$U\int_0^{2\pi}\frac{d\theta}{(2\pi)^2}\frac{\sqrt{2+\mu/(2t)}\cos(\theta-\alpha)}{\nu/|\mathbf{q}|-4t\sqrt{2+\mu/(2t)}\cos(\theta-\alpha)}=1. \tag{A13}$$

Since this integral does not depend on α, we can conclude that the zero sound velocity in the dilute limit does not depend on the direction of $\mathbf{q}$. This happens because the existence of a lattice is not important in such low electron concentrations.

Contrary to this, we can observe entirely opposite trends in the dilute doping regime ($n\sim 1$) in Fig. 8. In this regime, the zero sound velocity has almost no electron concentration dependence, but its $\mathbf{q}$ direction dependence becomes large. We avoid calculations around $n=1$, since we cannot apply the present RPA approximation at half-filling.

We shall now show analytically the n-independent behavior of v_{ZS}. When U is sufficiently small, the zero sound velocity is dominated by the pole $\nu-(\partial\varepsilon_{\mathbf{k}}/\partial\mathbf{k})\cdot\mathbf{q}=0$ of the integrand of Eq. (A6). Hence, in this case, v_{ZS} is obtained from

$$\frac{\nu}{|\mathbf{q}|}=\frac{\partial\varepsilon_{\mathbf{k}}}{\partial\mathbf{k}}\cdot\frac{\mathbf{q}}{|\mathbf{q}|}, \tag{A14}$$

with the constraint $\varepsilon_{\mathbf{k}}=\mu$ which comes from the integration range of Eq. (A6). On the other hand, we note that for the small $\mathbf{q}$ limit the particle-hole excitation energy $\nu(\mathbf{q})=\varepsilon_{\mathbf{k}+\mathbf{q}}-\varepsilon_{\mathbf{k}}$ becomes $\nu\sim(\partial\varepsilon_{\mathbf{k}}/\partial\mathbf{k})\cdot\mathbf{q}$, and the particle-hole condition $\varepsilon_{\mathbf{k}}<\mu<\varepsilon_{\mathbf{k}+\mathbf{q}}$ approaches $\varepsilon_{\mathbf{k}}\sim\mu$. Thus we can see that almost the whole possible range of Eq. (A14) is in the particle-hole excitation, and only the pole at the upper edge of the particle-hole excitation gives v_{ZS} in the weak-coupling limit. As a result, the zero sound velocity for the small U limit is obtained by the maximum value of the right-hand side of Eq. (A14) for a fixed $\mathbf{q}$,

$$v_{\mathrm{ZS}}=\max\left(\left.\frac{\partial\varepsilon_{\mathbf{k}}}{\partial\mathbf{k}}\right|_{\varepsilon_{\mathbf{k}}=\mu}\cdot\frac{\mathbf{q}}{|\mathbf{q}|}\right). \tag{A15}$$

We then obtain

$$v_{\mathrm{ZS}}=2\sqrt{2}t[\sin\{\arccos[\mu/(-4t)]\}], \tag{A16}$$

for the (1,1) direction, and

$$v_{\mathrm{ZS}}=\begin{cases} 2t & \text{for } \mu\leqslant -2t\\ 2t\,\sin\{\arccos[\mu/(-2t)-1]\} & \text{for } \mu>-2t \end{cases} \tag{A17}$$

for the (1,0) direction. These expressions are shown as the dashed curves in Fig. 8. For small dopings ($n\sim 1$, i.e., $\mu\sim 0$), v_{ZS} approaches $2\sqrt{2}t$ for the (1,1) direction and $2t$ for the (1,0) direction.

[1] N. E. Bickers, D. J. Scalapino, and S. R. White, Phys. Rev. Lett. **62**, 961 (1989).
[2] E. Dagotto, A. Moreo, F. Ortolani, D. Poilblanc, and J. Riera, Phys. Rev. B **45**, 10 741 (1992).
[3] P. W. Leung, Z. Liu, E. Manousakis, M. A. Novotny, and P. E. Oppenheimer, Phys. Rev. B **46**, 11 779 (1992).
[4] N. Bulut, D. J. Scalapino, and S. R. White, Phys. Rev. Lett. **72**, 705 (1994).
[5] N. Bulut, D. J. Scalapino, and S. R. White, Phys. Rev. Lett. **73**, 748 (1994).
[6] E. Dagotto, Rev. Mod. Phys. **66**, 763 (1994), and references therein.
[7] H. Eskes and R. Eder, Phys. Rev. B **54**, R14 226 (1996).
[8] A. Georges, G. Kotliar, W. Krauth, and M. J. Rozenberg, Rev. Mod. Phys. **68**, 13 (1996), and references therein.
[9] H. Matsumoto and F. Mancini, Phys. Rev. B **55**, 2095 (1997).
[10] R. Preuss, W. Hanke, C. Gröber, and H. G. Evertz, Phys. Rev. Lett. **79**, 1122 (1997).
[11] T. Saikawa, A. Ferraz, P. E. de Brito, and H. Kaga, Phys. Rev. B **56**, 4464 (1997).
[12] T. Tanamoto, K. Kuboki, and H. Fukuyama, J. Phys. Soc. Jpn. **60**, 3072 (1991).
[13] Z. Wang, Y. Bang, and G. Kotliar, Phys. Rev. Lett. **67**, 2733 (1991).
[14] T. Tohyama, P. Horsch, and S. Maekawa, Physica C **235–240**, 2231 (1994); Phys. Rev. Lett. **74**, 980 (1995).
[15] R. Eder, Y. Ohta, and S. Maekawa, Phys. Rev. Lett. **74**, 5124 (1995).
[16] D. K. K. Lee, D. H. Kim, and P. A. Lee, Phys. Rev. Lett. **76**, 4801 (1996).
[17] G. Khaliullin and P. Horsch, Phys. Rev. B **54**, R9600 (1996).
[18] L. Gehlhoff and R. Zeyher, Phys. Rev. B **52**, 4635 (1995).
[19] J. A. Hertz, Phys. Rev. B **14**, 1165 (1976).
[20] See, for example, E. Fradkin, *Field Theories of Condensed Matter Systems* (Addison-Wesley, New York, 1991).
[21] N. E. Bickers and D. J. Scalapino, Ann. Phys. (N.Y.) **193**, 206 (1989).
[22] See, for example, S. Doniach and E. H. Sondheimer, *Green's Functions for Solid State Physicists* (Addison-Wesley, New York, 1974).
[23] See, for example, W. Jones and N. H. March, *Theoretical Solid State Physics* (Dover, New York, 1973), Vol. 1.